

University of Dundee

ELIGULUM-A regulates lateral branch and leaf development in barley

Okagaki, Ron J.; Haaning, Allison; Bilgic, Hatice; Heinen, Shane; Druka, Arnis; Bayer, Micha

Published in:
Plant Physiology

DOI:
[10.1104/pp.17.01459](https://doi.org/10.1104/pp.17.01459)

Publication date:
2018

Document Version
Peer reviewed version

[Link to publication in Discovery Research Portal](#)

Citation for published version (APA):

Okagaki, R. J., Haaning, A., Bilgic, H., Heinen, S., Druka, A., Bayer, M., Waugh, R., & Muehlbauer, G. J. (2018). ELIGULUM-A regulates lateral branch and leaf development in barley. *Plant Physiology*, 176(4), 2750-2760. <https://doi.org/10.1104/pp.17.01459>

General rights

Copyright and moral rights for the publications made accessible in Discovery Research Portal are retained by the authors and/or other copyright owners and it is a condition of accessing publications that users recognise and abide by the legal requirements associated with these rights.

- Users may download and print one copy of any publication from Discovery Research Portal for the purpose of private study or research.
- You may not further distribute the material or use it for any profit-making activity or commercial gain.
- You may freely distribute the URL identifying the publication in the public portal.

Take down policy

If you believe that this document breaches copyright please contact us providing details, and we will remove access to the work immediately and investigate your claim.

Short Title

Regulation of Leaf and Lateral Branch Development

Gary J. Muehlbauer

Department of Agronomy and Plant Genetics, and Department of Plant and Microbial Biology,
University of Minnesota, St. Paul, MN 55108

ELIGULUM-A regulates lateral branch and leaf development in barley

Ron J. Okagaki¹, Allison Haaning¹, Hatice Bilgic¹, Shane Heinen¹, Arnis Druka², Micha Bayer²,
Robbie Waugh² and Gary J. Muehlbauer^{1,3}

¹Department of Agronomy and Plant Genetics, University of Minnesota, St. Paul, MN 55108

²The James Hutton Institute, Dundee, United Kingdom

³Department of Plant and Microbial Biology, University of Minnesota, St. Paul, MN 55108

One-sentence summary: The barley *ELIGULUM-A* gene regulates lateral branch development and acts to establish the blade–sheath boundary during leaf development.

Author contributions

R.J.O. performed most of the experiments and wrote the manuscript; A.H. performed the RNA *in situ* hybridizations and edited the manuscript; H.B.L. developed genetic materials; S.H. conducted the suppressor screen; A.D. performed the bioinformatics analysis; M.B. performed the bioinformatics analysis; R.W. oversaw the bioinformatics analysis and edited the manuscript; G.J.M. conceived the original research plan and edited the manuscript.

Funding information

Department of Agriculture-CSREES-NRI Plant Growth and Development program grant # 2004-03440, and funds received from the Triticeae Coordinated Agricultural Project, US Department of Agriculture/National Institute for Food and Agriculture grant number 2011-68002-30029 to G.J.M.

Corresponding author

G.J.M. muehl003@umn.edu

ABSTRACT

The shoot apical and axillary meristems control shoot development, effectively influencing lateral branch and leaf formation. The barley (*Hordeum vulgare* L.) *uniculm2* (*cul2*) mutation blocks axillary meristem development and mutant plants lack lateral branches (tillers) that normally develop from the crown. A genetic screen for *cul2* suppressors recovered two recessive alleles of *ELIGULUM-A* (*ELI-A*) that partially rescued the *cul2* tillering phenotype. Mutations in *ELI-A* produce shorter plants with fewer tillers and disrupt the leaf blade–sheath boundary, producing liguleless leaves and reduced secondary cell wall development in stems and leaves. *ELI-A* is predicted to encode an un-annotated protein containing a RNaseH-like domain that is conserved in land plants. *ELI-A* transcripts accumulate at the preligule boundary, the developing ligule, leaf margins, cells destined to develop secondary cell walls, and cells surrounding leaf vascular bundles. Recent studies have identified regulatory similarities between boundary development in leaves and lateral organs. Interestingly, we observed *ELI-A* transcripts at the preligule boundary, suggesting that *ELI-A* contributes to boundary formation between the blade and sheath. However, we did not observe *ELI-A* transcripts at the axillary meristem boundary in leaf axils, suggesting that *ELI-A* is not involved in boundary development for axillary meristem development. Our results show that *ELI-A* contributes to leaf and lateral branch development by acting as a boundary gene during ligule development but not during lateral branch development.

INTRODUCTION

Leaves and tillers, the vegetative branches that form at the base of grass plants, are key determinants of grass shoot architecture. Tillers develop from axillary meristems and undergo three distinct morphological stages: (1) initiation of an axillary meristem in the leaf axil; (2) development of leaf primordia on the axillary meristem to form an axillary bud; and (3) elongation of internodes into a tiller with the potential to form a grain-bearing spike (Schmitz and Theres, 2005). Primary tillers form in leaf axils on the main stem, and secondary and higher order tillers form in axils of leaves on primary tillers and subsequent tillers, respectively. Grass leaves develop from the flanks of the shoot apical meristem and axillary meristems, and are composed of a proximal sheath and distal blade divided by the ligular boundary. The ligular region is composed of the ligule, an outgrowth of an epidermal tissue flap, and the auricle. Auricles have two parts, a band of small cells separating the sheath from the blade and a flap of tissue growing out from the leaf margin that wraps around the stem in some species (Sylvester et al., 1990; Becraft et al., 1990). Both tillers and leaves are important agricultural traits for cereal crops and have been extensively studied (reviewed in Wang and Li, 2008; Lewis and Hake, 2015; Mathan et al., 2016). However, our understanding of the inter-relatedness of their genetic control is early in its fruition.

Positional information is important for morphogenesis and boundaries between cell types are often the location of new tissue development. Thus, the role of boundary formation in axillary meristem development is an intense area of study (reviewed in: Žádníková and Simon, 2014; Hepworth and Pautot, 2015; Wang et al., 2016). The *Arabidopsis thaliana* *REGULATORS OF AXILLARY MERISTEMS1* (*RAX1*) and *CUP-SHAPED COTYLEDON2* (*CUC2*) genes were identified by their expression pattern and reduced-branching mutant phenotypes, and were found to establish the boundary for axillary meristem development (Keller et al., 2006; Müller et al., 2006). Other boundary genes show the expected expression pattern but lack a clear axillary meristem phenotype in mutant plants. Plants over expressing *Arabidopsis* *BLADE-ON-PETIOLE* (*BOP*) show a branching phenotype, producing extra paraclades in leaf nodes (Ha et al., 2007). The role of *Arabidopsis* *LATERAL ORGAN FUSION* (*LOF1*) in axillary meristem development was revealed by double mutants with its homolog, *LOF2* (Lee et al., 2009). The *Arabidopsis* *REGULATOR OF AXILLARY MERISTEM FORMATION1* (*ROX1*) has a subtle phenotype but is involved in axillary meristem development (Yang et al., 2012). However, the role of *ROX1* in

axillary meristem development is more obvious in other species such as rice and maize, highlighting the importance of comparative work to fully delineate developmental pathways (Komatsu et al. 2003; Gallavotti et al. 2004). These studies, and others, have identified genes acting in axillary meristem boundary formation and it appears a number of these genes help establish other developmental boundaries.

Boundary formation is also critical for leaf patterning (reviewed in Bar and Ori, 2014; Lewis and Hake, 2015). Tomato plants produce compound leaves with several pairs of lateral leaflets and a terminal leaflet, with each leaflet having multiple lobes. *Goblet* (*Gob*) is one gene controlling this process, and *Gob* encodes a homolog of *CUC1/2* (Berger et al., 2009). *Gob* mutations also repress axillary meristem development (Busch et al., 2011). *Potato leaf* (*C*) and *blind* are recent duplications of the tomato *RAX1* homolog and sub-functionalization of these duplicated genes gave *blind* a role in axillary meristem development and *C* a role in leaf development (Busch et al., 2011). In *Arabidopsis*, *CUC2* functions similarly to produce serrated leaves (Nikovics et al., 2006; Bilsborough et al., 2010). It is now evident that many of the same genes act to establish boundaries for meristem and leaf development (Hepworth and Pautot, 2015; Wang et al., 2016)

The identification of genes with dual roles in boundary demarcation and leaf and axillary meristem development prompted Busch and colleagues (2011) to propose a conserved genetic system that establishes axillary meristems and determines leaf shape. A related genetic system for maize leaf and lateral organ initiation was recently proposed as well (Johnston et al., 2014). Transcriptome analysis of laser-dissected tissues from the maize preligule region identified genes expressed at the blade–sheath boundary that are homologs of previously identified genes involved in lateral organ initiation (Johnston et al., 2014). Among the differentially expressed genes were the maize *CUC2* and *BOP* homologs. RNA *in situ* hybridization experiments showed maize *CUC2-like* transcripts accumulating in the preligule band, the cleft of developing ligules, and at the location of lateral branch initiation. The maize *BOP-like* transcripts accumulated in developing ligules, leaf axils and axillary meristems (Johnston et al., 2014). The barley *UNICULME4* (*CUL4*) gene is the barley *BOP* homolog (Tavakol et al., 2015), and plants carrying mutations in *CUL4* are defective in both axillary meristem and ligule development. In addition, *CUL4* is expressed in developing ligules, leaf axils and axillary meristems, and defines

the boundaries of ligule and axillary bud development like the maize *BOP* homolog (Tavakol et al., 2015).

In this study, we conducted a genetic suppressor screen using a mutant that does not make tillers, *uniculm2* (*cul2*) (Babb and Muehlbauer, 2003), and identified two mutations in the *ELIGULUM-A* (*ELI-A*) gene that promoted axillary meristem development and tillering in the *cul2* mutant background. Mutations in *ELI-A* have been previously described as pleiotropic with altered ligule development, reduced plant height, weak culms, and compact spikes (Lundqvist and Franckowiak, 2002). Additional characterization showed that *eli-a* mutant plants exhibited reduced tillering and secondary cell wall formation compared with the non-mutant backcross parent line. We isolated the *ELI-A* gene and determined that it encodes a previously un-annotated protein. RNA *in situ* hybridizations showed that *ELI-A* transcripts are found in the preligular region, the developing ligule, leaf margins, cells destined to develop secondary cell walls, and in cells surrounding leaf vascular bundles. Taken together, these observations show that *ELI-A* plays a role in ligule and axillary meristem development. We propose that *ELI-A* functions in establishing a boundary during ligule development but not for axillary meristem development.

RESULTS AND DISCUSSION

Isolation and genetic characterization of *cul2* suppressor mutants

The barley *cul2* mutant rarely makes tillers due to its inability to produce axillary buds (Fig. 1; Babb and Muehlbauer, 2003). To identify suppressors of the *cul2* mutant phenotype, we mutagenized the Bowman-*cul2.b-rob1* stock. *Rob1* (*orange lemma*) is a phenotypic marker tightly linked to *cul2* (Franckowiak et al., 1997). Over 15,000 sodium azide-mutagenized, M₃ Bowman-*cul2.b-rob1* families were screened for plants that produced tillers and two recessive suppressor mutants were recovered. The two suppressors proved to be alleles of the previously described *ELI-A* gene (see below) and were named *eli-a.17* and *eli-a.18*. In Bowman-*eli-a.17; cul2.b-rob1* and Bowman-*eli-a.18; cul2.b-rob1* mutant plants, the unicum phenotype of *cul2* was partially suppressed (Fig. 1). For example, in a greenhouse trial, 28 of 41 Bowman-*eli-a.17; cul2.b-rob1* plants produced one or two tillers with the remaining plants having no tillers, and all 21 Bowman-*eli-a.18; cul2.b-rob1* plants had one or more tillers (Supplemental Fig. S1). Unexpectedly, homozygous mutant *eli-a.18* plants were short with leaves that drooped and lacked ligules (Fig. 1 and Fig. 2), whereas these traits were not seen in *eli-a.17* plants (Fig. 1 and Fig. 2).

To determine if *eli-a.17* and *eli-a.18* were allelic, seven crosses between Bowman-*cul2.b-rob1/cul2.b-rob1; eli-a.17/eli-a.17* and Bowman-*cul2.b-rob1/cul2.b-rob1; eli-a.18/eli-a.18* were made. Tillers were observed on 18 out of 19 F₁ plants, demonstrating that the two suppressors were allelic (Supplemental Fig. S2). In the F₂ plants, *eli-a.18* mutants exhibited stronger suppression of *cul2.b* than *eli-a.17*. Bowman-*eli-a.18; cul2.b-rob1* mutant plants were liguleless and developed an average of 2.9 tillers per plant compared with Bowman-*eli-a.17; cul2.b-rob1* that developed ligules and had 0.8 tillers per plant (Supplemental Fig. S1). Finally, the heteroallelic combination of *eli-a.17/eli-a.18* exhibited an intermediate number of tillers in the *cul2.b* mutant background, 1.59 tillers/plant, and an intermediate liguleless phenotype (Fig. 2, Supplemental Fig. S1 and Supplemental Fig. S3).

The *eli-a.17* and *eli-a.18* alleles also mapped to the same region on chromosome 2HS. We mapped *eli-a.17* using the *cul2* suppressor phenotype. The *eli-a.17; cul2.b-rob1* line was crossed with the cultivar Steptoe. The tightly linked *rob1* marker and a CAPS marker for SNP 1_0964 were used to identify 56 homozygous *cul2.b-rob1/cul2.b-rob1* F₂ plants (Supplemental

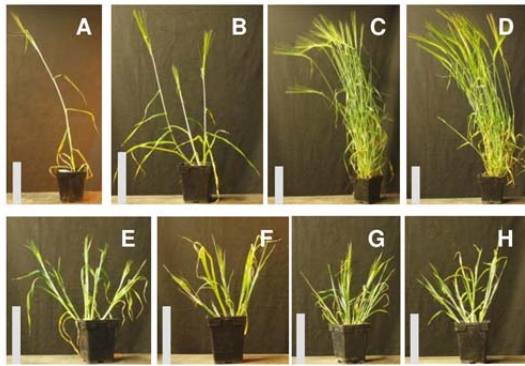


Figure 1: Mutant and non-mutant adult plant characteristics. A, Bowman-*cul2.b-rob1*. B, Bowman-*cul2.b-rob1; eli-a.17*. C, Non-mutant Bowman cultivar. D, Bowman-*eli-a.17*. E, Bowman-*eli-a.18*. F, Bowman-*cul2.b-rob1; eli-a.18*. G, *eli-a.14*. H, *cul2.b-rob1; eli-a.14*. The non-mutant Bowman and Bowman-*eli-a.17* plants in panels C and D were grown in the field and transferred to pots for pictures. Other plants were grown in a growth chamber. Bar = 20 cm.

Table S1). The *eli-a.17* phenotype of these 56 individuals was determined in F₃ families, because the suppressor phenotype is not fully penetrant and some F₂ *eli-a.17/eli-a.17; cul2.b-rob1/cul2.b-rob1* plants were unicum. *Eli-a.17* mapped 2.2 cM proximal of SNP 2_0964 at map position 17.85 on the SNP map (Supplemental Fig. S4). *Eli-a.18* was mapped using the liguleless phenotype in 220 F₂ individuals from a cross between Bowman-*eli-a.18; cul2.b-rob1* and the cultivar Harrington. The liguleless trait was mapped 1.6 cM proximal to SNP 3_1284 at position 19.47 on 2HS (Supplemental Fig. S4).

Barley *eli-a* mutants were previously described as recessive mutations producing a phenotype of dwarfed liguleless plants with weak culms that break at the nodes (Lundqvist and Frankowiak, 2002). We observed these characteristics in the *eli-a.18* mutant. In addition, the attachment of outer tillers to the crown was so poor that tillers leaned outwards (Fig. 1). These similarities prompted us to test for allelism between *eli-a.18* and the previously described *eli-a* alleles. Six mutants classified as *eligulum* that had been backcrossed into the Bowman background were examined (Druka et al., 2011). Genetic stocks carrying three of the mutations *eli.12*, *eli-b.5*, and *eli-a.216* had few of the reported *eli-a* characteristics nor resembled either of our two suppressors and were not pursued. *Eli-a.3*, *eli-a.9*, and *eli-a.14* mutant stocks exhibited the short stature and liguleless characteristics of plants carrying the *eli-a.18* allele. An adult *eli-a.14* plant is shown in Figure 1, and the liguleless trait from *eli-a* plants is shown in Supplemental Figure S3. Three crosses of *eli-a.18* with *eli-a.3*, two crosses with *eli-a.9*, and one cross with *eli-a.14* were made. Ten F₁ plants were produced and they all exhibited short and liguleless mutant phenotypes. An example of the heteroallelic combination *eli-a.9/eli-a.18* is presented in Supplemental Fig. S2. These results confirm that our *cul2* suppressors are allelic with *eli-a* mutants.

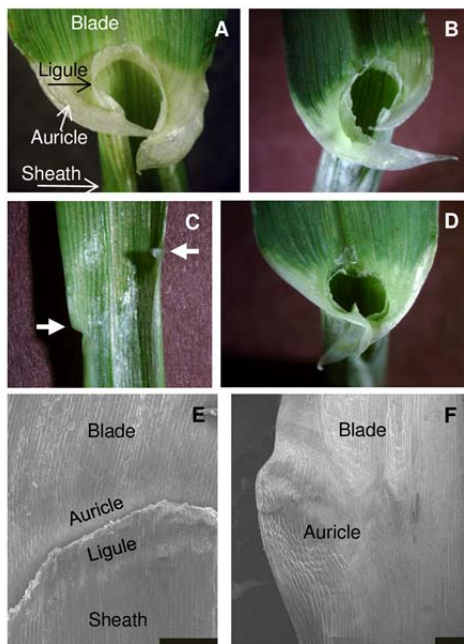


Figure 2: The ligular region in *eli-a* alleles. A – D, Ligules and auricles. A, Non-mutant Bowman. B, Bowman-*eli-a.17*. C, Bowman-*eli-a.18*, note the reduced auricles at the leaf margin, indicated by the arrows and the absence of the ligule. D, Heterozygous Bowman-*eli-a.17/eli-a.18*, note the reduced ligule and auricle development. E – F, scanning electron microscopy of the ligular regions. E, Non-mutant Bowman, the ligule has been trimmed back to uncover the underlying auricle. F, Bowman-*eli-a.18* ligular region. Scale bar = 200 μ m

To determine if *eli-a.3*, *eli-a.9*, and *eli-a.14* suppress the *cul2* unculm phenotype, we crossed *eli-a.3*, *eli-a.9*, and *eli-a.14* with Bowman-*cul2.b-rob1*. In total, 23 mutant plants were recovered (*eli-a.3/eli-a.3; cul2.b-rob1/cul2.b-rob1*, *eli-a.9/eli-a.9; cul2.b-rob1/cul2.b-rob1*, and *eli-a.14/eli-a.14; cul2.b-rob1/cul2.b-rob1*) and 22 of 23 individuals developed tillers. Examples of suppression of *cul2.b* by *eli-a.14* and *eli-a.9* are shown in Figure 1 and Supplemental Figure S2. All five *eli-a* alleles tested suppress *cul2*, thereby establishing a role for *ELI-A* in axillary meristem development.

Axillary bud and tiller development in *eli-a* mutants

To study the impact of *eli-a* on early axillary bud development, we examined seven-day-old shoot apices from Bowman-*eli-a.17; cul2.b-rob1*, Bowman-*cul2.b-rob1*, Bowman-*eli-a.17*, and the non-mutant Bowman cultivar. Despite being a weak allele, the *eli-a.17* allele was used for this experiment because germination rates were higher and growth more uniform than other *eli-a* alleles. Two to three primary axillary buds were typically seen in non-mutant Bowman seedlings at seven days (Fig. 3). In these experiments, no axillary buds were seen in *cul2.b* seedlings (Fig. 3), but in previous experiments occasionally an axillary meristem would develop but would be blocked from forming an axillary bud (Babb and Muehlbauer, 2003). One to two primary axillary buds were present in seven-day-old Bowman-*eli-a.17* seedlings (Fig. 3). In the

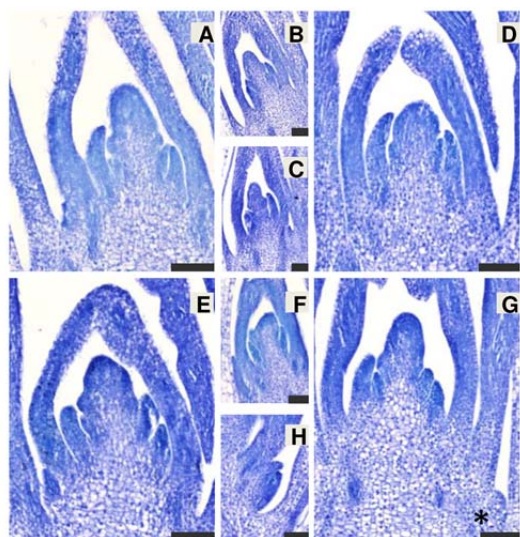


Figure 3. Longitudinal sections of seven-day-old shoot apices from non-mutant and mutant lines stained with Toluidine Blue. Axillary buds are shown in their own panels as median sections of the shoot apex generally do not capture the axillary buds. A, Non-mutant Bowman shoot apical meristem. B, Bowman axillary bud #3. C, Bowman axillary bud #2. D, Bowman-*cul2.b-rob1* shoot apical meristem. E, Bowman-*eli-a.17* shoot apical meristem. F, Bowman-*eli-a.17* axillary bud. G, Bowman-*eli-a.17; cul2.b-rob1* shoot apical meristem, the edge of a small axillary bud is visible at the lower right (*). H, Section through axillary bud #1 seen in panel G. Size bar = 100 μ m.

Bowman-*eli-a.17; cul2.b-rob1* material, zero to two axillary buds were visible at seven days (Fig. 3). A seven-day-old Bowman-*eli-a.18* shoot apex is shown in Supplemental Figure S5 for comparison.

The rates of axillary bud and tiller development between the *eli-a.17* mutant and non-mutant were compared, and the numbers of tillers on adult plants for *eli-a.17* were compared to the non-mutant. Developing axillary buds and tillers were counted weekly in dissected seedlings of *eli-a.17* and non-mutant plants at two weeks through six weeks after planting. Over this period, the rate of axillary bud and tiller emergence was significantly slower in *eli-a.17* plants than in non-mutant plants (Supplemental Fig. S6).

Tiller numbers on field-grown plants were determined for both Bowman-*eli-a.17* and Bowman-*eli-a.18* plants. At maturity, plants carrying the strong mutant allele, *eli-a.18* had approximately half as many tillers as non-mutant plants, whereas plants carrying the weak *eli-a.17* allele had approximately 20% fewer tillers than non-mutant plants (Table 1). This small reduction in tillering in *eli-a.17* compared to non-mutant Bowman was consistent with tiller numbers counted from individual families in previous seasons. For example, non-mutant Bowman plants had an average of 45.5 (S.E. = 3.40) tillers per plant and an adjacent family of Bowman-*eli-a.17* plants had 33.9 (S.E. = 3.41) tillers per plant in the 2013 field. The reduced tiller number in *eli-a.17* and *eli-a.18* mutants compared to non-mutant and the increase in tiller number in *cul2.b, eli-a double* mutants indicates that the mechanism controlling rate of tillering

and adult tiller number is not necessarily the same mechanism that suppresses the *cul2* mutant phenotype.

Ligule and auricle development in *eli-a* mutants

The grass leaf sheath–blade boundary is marked by two structures, the ligule and auricle (Fig. 2). The auricle can be divided into two parts, a band of small, light colored cells separating the blade from the sheath and a flap of tissue growing out from the leaf margin that often wraps around the stem (Fig. 2). The boundary runs perpendicular to the long axis of the leaf, and the paired auricle flaps are usually directly opposite of each other.

Ligules and the bands of auricle cells were generally not visible in *eli-a.18* plants, but small auricle flaps were present (Fig. 2). Figure 2 presents an adaxial view of the ligular region from a non-mutant plant with the ligule cut away to show the underlying auricle cells. A small auricle develops in *eli-a.18* plants at the leaf margin and extends a short distance inward (Fig. 2; Supplemental Fig. S3). Ligules were not obvious in most plants, although small rudimentary ligules have been seen. When present, rudimentary ligules were short and did not span the width of the leaf (Supplemental Fig. S3).

A range of ligule and auricle development was seen in the five *eli-a* alleles. Ligule and auricle development was visibly disrupted in *eli-a.3*, *eli-a.9*, *eli-a.14*, and *eli-a.18* leaves (Supplemental Fig. S3). Ligules and auricles appeared normal in homozygous *eli-a.17* plants (Fig. 2 and Supplemental Fig. S3). However, heterozygous *eli-a.17/eli-a.18* plants have small ligules, while heterozygous *eli-a.18/ELI-A* plants produce normal ligules indicating that the *eli-a.17* allele is not equivalent to the non-mutant allele for ligule development (Fig. 2 and Supplemental Fig. S3).

Another characteristic of leaf development in *eli-a* mutants was the displacement of the blade–sheath boundary as indicated by the placement of auricle flaps at the leaf margin (Supplemental Fig. S3). In non-mutant plants, these structures are opposite one another on the leaf, and the blade–sheath boundary runs approximately perpendicular to the longitudinal axis of the leaf (Fig. 2 and Supplemental Fig. S3). Displacement of the blade–sheath boundary was commonly observed in *eli-a.3*, *eli-a.9*, *eli-a.14*, and *eli-a.18* (Supplemental Fig. S3). This aberrant boundary positioning was infrequent with non-mutant and *eli-a.17* leaves.

Inflorescence development

Eli-a mutant spikes have a compact appearance with spikelets packed tightly together, particularly towards the tip (Supplemental Fig. S7; Lundqvist and Franckowiak, 2002). This characteristic is less obvious in weaker alleles like *eli-a.3* and *eli-a.17* (Supplemental Fig. S7). The *cul2* mutation produces spikes with spikelets irregularly placed along the spike, particularly near the tip (Babb and Muehbauer, 2003). Expression of these traits in double mutant *eli-a; cul2.b* plants range from compact spikes with an irregular arrangement of spikelets to severe disruption of spikelet formation (Supplemental Fig. S7). Thus, although the *eli-a* mutation partially suppresses the axillary meristem defect in *cul2* mutants, the *cul2* spike phenotype is not suppressed.

Secondary cell wall defects in *ELI-A* mutants

Non-mutant leaves from the Bowman cultivar have midrib, leaf margin, and bundle sheath extension cells with thick secondary cell walls providing strength to the leaves. Stained with Safranin O, these cells appeared small with thick red cell walls (Fig. 4). Corresponding cells in Bowman-*eli-a.18* leaves were larger with thin cell walls (Fig. 4). Safranin O stains lignin, and the weaker staining seen in *eli-a.18* suggests reduced lignin content in *eli-a.18* (Ruzin, 1999). These changes may explain the lack of structural strength and tendency to droop downward in mutant leaves (Fig. 4). *ELI-A* apparently has a similar function in other tissues. Epidermal cells in the culm and cells immediately under the epidermis have thick cell walls in non-mutant plants (Supplemental Fig. S8). The corresponding cells from *eli-a.18* and *eli-a.3* mutant culms have thin cell walls (Supplemental Fig. S8). This may explain the weakness reported in *eli-a* culms (Lundqvist and Franckowiak, 2002). However, secondary cell walls did develop in the xylem and other cells within vascular bundles in *eli-a.18* mutant plants, demonstrating that *ELI-A* is not an absolute requirement for secondary wall development (Fig. 4).

Disrupting cell wall development may explain other characteristics of *eli-a* mutants. In *eli-a.18* mutant plants, secondary cell wall formation in the mestome sheath and bundle sheath extensions was greatly reduced. Structural strength is but one function of secondary cell walls (reviewed in Leegood, 2008). Fricke (2002) proposed that the bundle sheath regulates the flow of water and photosynthate between the leaf mesophyll and the vascular system. Other work suggests bundle sheath extensions are an adaptation for desiccation stress (Kenzo et al., 2007).

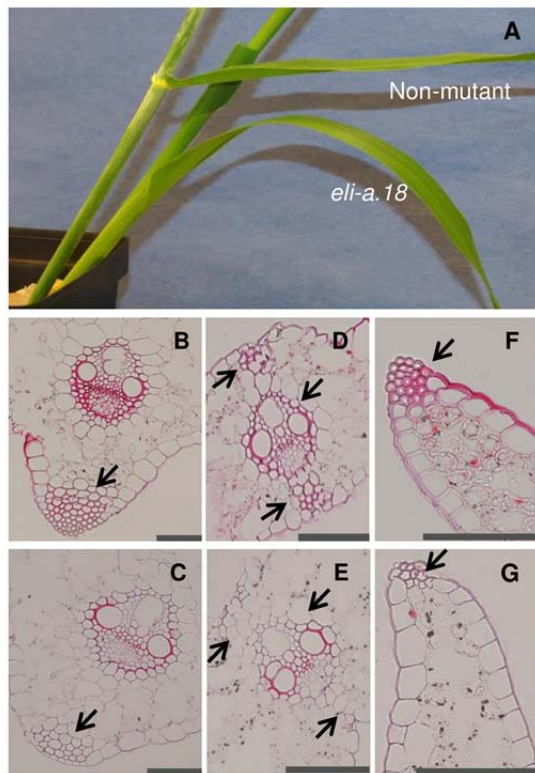


Figure 4. Secondary cell wall development. A, Comparison of leaves from mature non-mutant Bowman and Bowman-*eli-a.18* plants. B-G are Safranin-O stained. B, Midrib from non-mutant plant. C, Midrib from Bowman-*eli-a.18* plant. D, Leaf vein from non-mutant plant. E, Leaf vein from Bowman-*eli-a.18* plant. F, Leaf margin from non-mutant plant. G, Leaf margin from Bowman-*eli-a.18* plant. Arrows point to cell wall differences in the leaf midrib (B, C), the bundle sheath extension and mestome sheath (D, E), and the leaf margin (F, G). Scale bar = 100 μ m.

Physiological limitations imposed by mutant cell walls could explain the semi-dwarf stature and reduced rate of tillering in *eli-a* plants, but would not account for the suppression of the *cul2* axillary meristem trait. However, cell wall stiffness in the shoot apex influences auxin transport, *CUC3* expression, and leaf primordia emergence in other systems and provides a plausible mechanism for controlling axillary meristem development (Kierzkowski et al., 2012; Nakayama et al., 2012; Fal et al., 2016).

Isolation and characterization of the *ELI-A* gene

The *ELI-A* gene was identified by comparing the transcriptomes of the sodium azide-generated *eli-a.17* and *eli-a.18* mutant alleles against non-mutant plants. RNA was isolated and sequenced from two-week-old seedling crown tissue from Bowman, Bowman-*cul2.b*, Bowman-*cul2.b-rob1*, Bowman-*eli.a-17*, Bowman-*cul2.b-rob1; eli.a-17*, Bowman-*eli.a.18* and Bowman-*cul2.b-rob1; eli.a.18*. *De novo* assembly of sequence reads from the Bowman line produced 31,976 transcripts (Supplemental Data S1). SNPs were then identified between non-mutant Bowman and the mutant lines. These SNPs would include any existing variation in the Bowman lines and mutations induced by the sodium azide treatment, including the causative mutations for

eli-a.17 and *eli-a.18* (Supplemental Tables S2–S7). Transcript11292 (Supplemental Data S1) contained a SNP at position 1103 from the Bowman-*cul2.b-rob1; eli-a.17* and Bowman-*eli.a.17* lines and a different SNP at position 796 in the Bowman-*cul2.b-rob1; eli-a.18* and Bowman-*eli.a.18* lines (Supplemental Tables S2–S5). These two SNPs in Transcript11292 were not present in the Bowman, Bowman-*cul2.b-rob1* progenitor line, or the related Bowman-*cul2.b* line, providing evidence that the sequence differences were not pre-existing polymorphisms (Supplemental Tables S6, S7). Both SNPs were confirmed by Sanger sequencing PCR products from the Bowman, Bowman-*cul2.b-rob1; eli-a.17* and Bowman-*cul2.b-rob1; eli-a.18* genomic DNAs.

A full-length cDNA sequence, AK375036, matching Transcript11292 was identified in a BLASTn search of the GenBank non-redundant sequence database. The entire predicted coding region of AK375036 was sequenced from the *eli-a.17*, *eli-a.18*, *eli-a.3*, *eli-a.9*, and *eli-a.14* alleles (Fig. 5). Foma, the progenitor allele of *eli-a.3* and *eli-a.9*, Kristina, the progenitor allele of *eli-a.14*, the Bowman-*cul2.b-rob1* line, progenitor of *eli-a.17* and *eli-a.18*, and the backcross parent Bowman were also sequenced. *Eli-a.3*, *eli-a.9*, and *eli-a.17* contained the non-conservative amino acid substitutions proline to serine, threonine to isoleucine, and aspartic acid to a tyrosine, respectively. The *eli-a.14* and *eli-a.18* alleles contained nonsense mutations. This cDNA corresponds to gene model MLOC_58453 from the barley genome (International Barley Genome Consortium, 2012).

MLOC_58453 co-segregated with the liguleless phenotype in the *eli-a.18* mutant and the *eli-a.17* suppressor phenotype in the mapping populations described above. MLOC_58453 was mapped in the Bowman-*cul2.b-rob1; eli-a.18* Harrington F₂ population using a CAPS marker targeting the mutated base pair (Supplemental Table S1). As expected, all liguleless plants were homozygous for the mutant MLOC_58453 CAPS allele (Supplemental Fig. S4). Similarly, a SNP located within the MLOC_58453 coding region co-segregated with the suppressor phenotype in the *eli-a.17* mapping population (Supplemental Fig. S4 and Supplemental Table S1). MLOC_58453 has been mapped to chromosome 2HS on the barley genome assembly (The International Barley Genome Consortium, 2012).

***ELI-A* is a conserved plant gene containing a RNaseH-like domain**

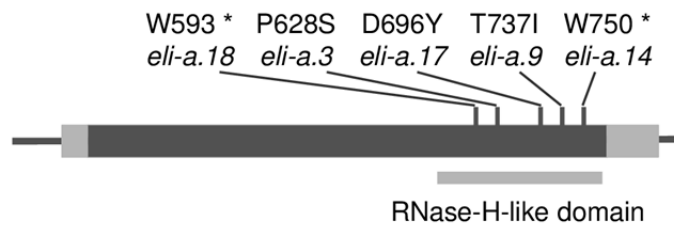


Figure 5. The *ELI-A* gene and location of mutations. The dark grey box indicates the single exon in the gene, and lighter grey boxes mark the 5' and 3' untranslated regions. Mutations in *eli-a.14* and *eli-a.18* created stop codons. Prediction programs Phyre², LOMETS, and InterProScan 5 identified a RNaseH-like domain at the carboxy end of the peptide.

Homologous *ELI-A* sequences were found in land plants ranging from *Arabidopsis thaliana* and rice, to the non-vascular and primitive vascular plants, *Physcomitrella patens* and *Selaginella moellendorffii* (Supplemental Table S8). A distantly related sequence was present in the green algae *Chlamydomonas reinhardtii*. Mutant phenotypes in *Arabidopsis thaliana* have not been reported in TAIR, and the two homologs, AT1G12380 and AT1G62870, are described as hypothetical proteins (<https://www.arabidopsis.org/>, May 2017). Nor are the maize gene models homologous with *ELI-A* associated with a maize phenotype or classical gene (<http://maizegdb.org/>, May 2017). A phylogenetic tree developed from these sequences is presented in Supplemental Figure S9. Despite the sequence conservation there is a lack of evidence for *ELI-A* function outside of barley.

We examined peptide sequences of the barley *ELI-A* protein and in homologous rice and *Arabidopsis* proteins. The peptides from barley, rice, and *Arabidopsis* were predicted by Phyre², LOMETS, and InterProScan 5 to contain a ribonuclease H-like domain (Kelley and Sternberg, 2009; Wu and Zhang, 2007; Quevillon et al., 2005). InterProScan 5 did provide additional details, but Phyre² and LOMETS identified the putative ribonuclease H-like domain as a member of the Hermes transposase class. The Hermes class of RNaseH-like domains is found in hAT

family transposons; hAT family transposons also contain an N-terminal BED-type zinc finger and the hAT domain (Hickman et al., 2005).

Further examination of the relationship of the ELI-A protein to members of the RNase H-like superfamily found that the Hermes domain is a class I RNaseH that is within clade B under the classification scheme of Majorek et al. (2014). This family is mainly composed of transposases with endonuclease activity, although one member of clade B encodes the human P52^{rIPK} protein that regulates a human RNA-dependent serine/threonine protein kinase (Gale et al., 2002). Phyre² detected BED-type zinc fingers in the rice and Arabidopsis peptides with moderate confidence. However, the hAT domain was not detected by Phyre², LOMETS, or InterProScan 5 in barley, rice or Arabidopsis. At present, the origin of *ELI-A* from a transposon is not known.

***ELI-A* expression pattern**

Expression levels of *ELI-A* from eight tissues were calculated from previously published RNAseq data (The International Barley Genome Consortium, 2012). At this level of resolution, expression was highest in 5 and 15 mm long immature inflorescences (Supplemental Fig. S10). *ELI-A* expression levels were low in most other tissues. RNA was extracted from axillary buds, 5-mm long inflorescences, and leaf blades for RT-qPCR to validate the RNAseq data. Transcript levels were highest in the inflorescence, while transcript levels were below the threshold of detection in leaf tissue consistent with results from the RNAseq data (Supplemental Fig. S10).

RNA *in situ* hybridizations were performed to further refine the distribution of *ELI-A* transcripts. In non-mutant, four-day-old shoot apices, expression was strong in leaf midribs, along the leaf margin, the bundle sheath surrounding vascular bundles, and in bundle sheath extension cells (Fig. 6). A sense control is shown in Supplemental Figure S11. *ELI-A* transcripts were detected in similar locations in *cul2.b* mutant seedlings (Fig. 6). In transverse *cul2.b* sections, expression was detected in small clusters of cells along the abaxial leaf surface (Fig. 6). Expression at this location was variable and was also seen in non-mutant plants (Supplemental Fig. S11). There were no consistent differences in expression between non-mutant and *cul2.b* plants.

ELI-A transcripts are present in developing ligules. A low level of *ELI-A* transcripts was found in emerging ligules (Fig. 6 and Supplemental Fig. S11), but not in older ligules (Fig. 6).

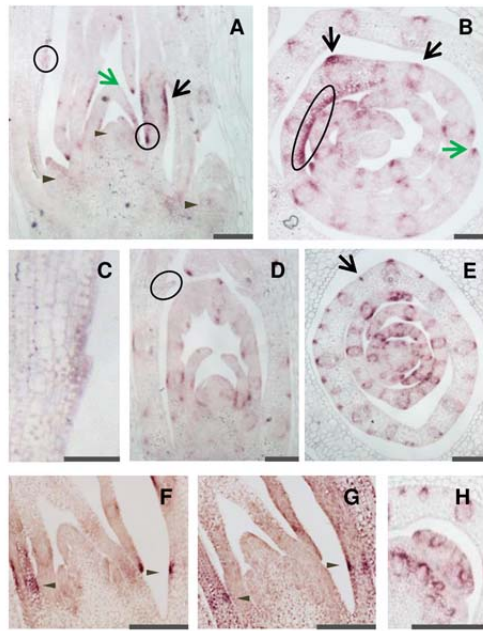


Figure 6. *ELI-A* expression in non-mutant and *cul2.b* seedlings. A-C, Four-day-old non-mutant shoot apex probed with an antisense *ELI-A* probe. A, Longitudinal section showing little staining in or adjacent to the shoot apical meristem and axillary buds, indicated by triangles. Short patches of staining at the adaxial and abaxial sides of leaves were occasionally seen (dark arrow); this pattern is likely from vascular bundles as seen in panels B and H. Staining was observed in newly forming ligules and leaf primordia that may represent developing ligules (circled). Leaf margins were also stained (green arrow). B, Transverse section showing staining in leaf margins, midribs, and around vascular bundles. Staining along a portion of the adaxial side of a developing leaf, circled, can be followed across the leaf in serial sections, and may be associated with the developing ligules. C, Close-up view of ligule circled in panel A. D-E, four-day-old *cul2.b* shoot apex probed with an antisense *ELI-A* probe. D, Longitudinal section of a *cul2.b* shoot. E, Transverse section of a *cul2.b* shoot. *ELI-A* staining pattern was similar to non-mutant shoot apices; the variable staining in small clusters of cells along the abaxial leaf surface (arrow) was seen in non-mutant plants (Supplemental Fig. S11); transcript was not detected in the older ligules (circled). F – G, Serial sections of four-day-old shoot probed for *ELI-A* or *HvLg1*. F, *ELI-A* staining was observed in the same location as the adaxial *HvLg1* staining. G, *HvLg1* staining was detected on the adaxial and abaxial surfaces. H, *ELI-A* expression in leaf axils and axillary buds is associated with vascular bundles. Scale bar = 100 μm in panel C, and 200 μm in other panels.

In younger leaf primordia, a prominent signal was present slightly above the base of leaf primordia on the adaxial side in longitudinal sections. This signal appeared to correspond to the band of expression found on the adaxial surface of leaf primordia in transverse sections (Fig. 6). A serial section from higher up along this shoot apex showed expression continuing along the adaxial surface (Supplemental Fig. S11). This is the expected location of the preligule band, which marks the boundary between the blade and sheath. To verify this, we looked at the expression of the barley homolog of the maize *Liguleless1* (*Lg1*) gene. The maize *Lg1* gene is expressed at the preligule band at the blade–sheath boundary (Moon et al., 2013). *ELI-A* and *HvLGI* transcripts were both found on the adaxial surface of the blade–sheath boundary in serial sections from the same shoot apex (Fig. 6). A *HvLGI* sense control is shown in Supplemental Figure S11. Taken together, these results indicate that *ELI-A* acts like a boundary gene in the development of the blade–sheath boundary.

Weak staining was sometimes seen in axillary buds and in leaf axils adjacent to developing axillary meristems, as well as within axillary buds in longitudinal sections (Fig. 6 and

Supplemental Fig. S11). In transverse sections, this transcript appeared to associate with developing vascular bundles rather than the leaf axil or axillary meristem (Fig. 6). *ELI-A* expression further down the shoot apex where the axillary bud emerged from the shoot apex was very weak compared to expression around vascular bundles higher up the shoot apex (Supplemental Fig. S11). The expression pattern of *ELI-A* did not indicate a direct function in boundary formation or stem cell maintenance.

Sclerenchyma cells are found in developing leaf ribs, hypodermal sclerenchyma cells, and leaf margins from barley plants (Wenzel et al., 1997; Trivett and Evert, 1998). These are locations where *ELI-A* transcripts were detected in leaf primordia. In *eli-a.18* mutants, cells comprising midribs have thin cell walls and lack the thick secondary cell walls of normal rib cells. Elsewhere in the leaf and in the culm, *ELI-A* transcripts coincided with cells having thickened secondary cell walls (Fig. 5 and Fig. 6). *ELI-A* transcripts were not detected in the xylem or phloem (Fig. 6 and Supplemental Fig. 11). This absence of secondary cell walls can explain the weak leaves and culms in *eli-a* mutant plants. However, the absence of *ELI-A* transcripts in leaf axils from both *CUL2* and *cul2.b* plants argues against a direct role for secondary cell walls in the suppression of the *cul2* tillering phenotype by *eli-a*.

***ELI-A* acts like a boundary gene in the leaf but not in the leaf axil**

A conserved set of genes are believed to control leaf and axillary meristem development. In tomato and other eudicots, development of leaf serrations, leaflets, and axillary meristems in leaf axils are regulated by *CUC*, *RAX*, and *LATERAL SUPPRESSOR* (Busch et al., 2011). Grass leaves lack serrated margins and leaflets common in eudicots, but there is a boundary between the blade and sheath consisting of the ligule and auricles (Langdale, 2005; Lewis and Hake, 2015). Laser microdissection transcriptome analysis showed maize *CUC2*, *BOP*, and *ELI-A* homologs upregulated at the blade–sheath boundary (Johnston et al., 2014). *In situ* hybridizations confirmed the maize *CUC2* and *BOP* expression in newly forming ligules at the leaf blade - sheath and axillary meristem boundaries (Johnston et al., 2014). Barley *CUL4* and maize *BOP* are homologous genes. This postulated genetic system may derive from a common evolutionary origin for leaves and axillary meristems as suggested by Busch and colleagues (2011), and is consistent with expectations from the barley phytomer model proposed by Forster

and co-workers (2011). Alternatively, the conserved genes may be part of a conserved genetic module that acts in leaf and axillary meristem development (Carroll, 2008).

This system of genes is expected to function in barley development. The barley *BOP* homolog, *CUL4*, is expressed in newly formed ligules at the blade–sheath junction and at axillary meristem boundaries in leaf axils (Tavakol et al., 2015). However, *CUL4* is expressed in developing ligules and does not appear to specify the location of the blade-sheath boundary (Tavakol et al., 2015). Like *CUL4*, *ELI-A* is expressed in newly forming ligules, but is also expressed earlier in development than *CUL4* where its expression pattern overlaps the barley homolog of the maize *Lg1* gene in the preligular region separating the blade from sheath (Moon et al., 2013). In addition, the *ELI-A* mutants (*eli-a.9*, *eli-a.3*, *eli-a.14* and *eli-a.18*) exhibiting a liguleless phenotype also exhibit a disrupted blade–sheath boundary (Supplemental Fig. S3). Taken together, our results show that *ELI-A* and *CUL4* are both necessary to produce a ligule, with *ELI-A* acting at a similar time and place with *HvLg1* to establish the leaf blade–sheath boundary.

CUL4 and *ELI-A* both have roles in axillary meristem development. However, their roles in axillary development appear different because the *cul4* and *eli-a* tillering phenotypes share few characteristics. The *cul4* mutation restricts axillary meristem development to a short developmental window; new axillary buds cease appearing after three to four weeks in *cul4.5* plants (Tavakol et al., 2015). The *eli-a* mutation slows the rate of axillary meristem development. Furthermore, *eli-a* mutants suppress the low-tillering *cul2* phenotype; *cul4* does not (Babb and Muehlbauer, 2003).

RNA *in situ* hybridization provided further evidence for differing roles for *ELI-A* during leaf and axillary branch development. The *ELI-A* transcripts were present at the leaf blade–sheath boundary where it participates in ligule development. Although *ELI-A* transcripts were occasionally detected in or adjacent to developing axillary buds in longitudinal sections, *ELI-A* was shown in transverse sections to be closely associated with vascular bundles rather than organ boundaries or meristematic regions. This expression pattern in the leaf axil was not similar to other characterized axillary meristem boundary genes including *CUL4* and the rice *CUC3* and *RA2* homologs (Tavakol et al., 2015; Oikawa and Kyoizuka, 2009). It is possible that transient *ELI-A* expression in axillary meristems or organ boundaries was not detected, or the *ELI-A* protein is transported as shown for the rice *LAX* protein (Oikawa and Kyoizuka, 2009). While

acknowledging these possibilities, our data support a model where *ELI-A* has an early role and *CUL4* has a later role in creating the blade–sheath boundary during leaf development. However, during axillary meristem development, *CUL4* is expressed in the leaf axil and plays a role in boundary formation. While *ELI-A* does not appear to be expressed in the leaf axil boundary, it still has a role in axillary meristem development. Taking these findings together, we propose that *ELI-A* acts like a boundary gene at the leaf blade-sheath boundary and promotes secondary cell wall formation in leaves and other tissues, but acts in an unknown manner during axillary meristem development.

MATERIALS AND METHODS

Plant materials and populations:

Mutant alleles *cul2.b*, *eli-a.3*, *eli-a.9*, *eli-a.14*, and *rob1* were obtained from the collection of mutants backcrossed to the cultivar Bowman (Druka et al., 2011). Plants were either field grown, or grown under controlled conditions in a greenhouse or growth chamber with 16 hours of light at 22 °C and 8 hours dark at 18 °C. Supplemental Table S9 provides information on the mutant alleles and barley cultivars used here.

The *cul2* suppressor screen was conducted by mutagenizing Bowman-*cul2.b-rob1* grain. The *rob1* allele is approximately 2 cM from *cul2* and produces an orange lemma phenotype that was used to track the tightly linked *cul2.b* allele. Approximately 20,000 Bowman-*cul2.b-rob1* kernels were treated with sodium azide according to the protocol described in Döring et al. (1999). From the M₂ plants, over 15,000 M₃ families (~70,000 plants) were produced and screened. M₃ families segregating for plants with tillers were identified. Families were re-tested for the suppressor phenotype in subsequent generations.

To recover homozygous *eli-a.17* plants, we conducted a single backcross of *eli-a.17/eli-a.17; cul2.b-rob1/cul2.b-rob1* plants to the non-mutant Bowman cultivar and self-pollinated an F₁ plant to generate an F₂ population. Families derived from phenotypically non-mutant F₂ plants were screened in the F₃ and F₄ generations to recover homozygous *eli-a.17/eli-a.17* and *eli-a.17/eli-a.17; cul2.b-rob1/cul2.b-rob1* lines (Supplemental Fig. S12). *Eli-a.18* mutant plants were identified by their short stature and liguleless leaves. F₂ populations segregating *eli-a.17* and *eli-a.18* were produced by crossing the Bowman-*eli-a.18; cul2.b-rob1* line with the non-mutant cultivar Harrington, and by crossing the Bowman-*eli-a.17; cul2.b-rob1* line with the non-mutant cultivar Steptoe.

Seedling tests for suppression of *cul2.b* by *eli-a.3*, *eli-a.9*, and *eli-a.14* were performed by crossing the mutants and recovering *eli-a/+; cul2.b/cul2.b* individuals. These plants were allowed to self-pollinate. Tillering phenotypes of suppression of *cul2* by *eli-a.3* and *eli-a.14* were scored in the growth chamber in three to four-week-old F₂ plants. Suppression of *cul2.b* by *eli-a.9* was tested in field grown F₂ families.

Morphological characterization

Shoot apices from one-week-old seedlings were sectioned and stained to examine axillary bud development as previously described (Babb and Muehlbauer, 2003). Axillary buds and tillers were counted on growth chamber grown plants, weeks two through six. Three replicates, three plants per replication, were counted at each time point; at least eight plants were examined in all but two time points. Leaves were removed to count axillary buds and tillers. Axillary buds were further classified as primary axillary buds, those growing in leaf axils, and secondary axillary buds, those growing in tiller axils (Dabbert et al., 2010). Tiller number was determined from field grown plants at four weeks, six weeks, and at maturity; five plants per replicates with six replicates of non-mutant and Bowman-*eli-a.17*, and five replicates of Bowman-*eli-a.18* were randomized in the field.

Ligular regions were examined on four to six-week-old plants grown in the growth chamber or greenhouse. Development of ligules, auricles, and other features were characterized from the second or third leaf. The leaf blade-sheath junction region was photographed under low-power light microscopy and with cryo-scanning electron microscopy. Scanning electron microscopy was performed on a Hitachi S3500N scanning electron microscope at 5 or 10 kV (Ahlstrand, 1996).

For histological work, plant tissues were fixed in paraformaldehyde and embedded in paraffin (Javelle et al., 2011). Sections were stained with Toluidine Blue or Safranin O (Humason, 1979; Ruzin, 1999). RNA *in situ* hybridizations were performed as described by Javelle et al., (2011). Probes for RNA *in situ* hybridizations were developed from PCR amplicons from genomic DNA using primers ELI-1393F and ELI-1877R or HvLG1-79F and HvLG1-598R, cloned into pGEM-T Easy (Promega, Madison, WI). Plasmids were used as templates for PCR with M13 forward and reverse primers. RNA was synthesized from resulting amplicons with SP6 or T7 RNA polymerase to make the sense and antisense probes using the Roche DIG RNA Labeling Kit (Sigma-Aldrich, St. Louis, MO).

Molecular biology procedures

Procedures for DNA isolation, PCR, Cleavage Amplified Polymorphic Sequence (CAPS) markers, and other routine molecular techniques were described previously (Dabbert et al., 2010). PCR primers (Supplemental Table S10) were developed using the program Primer3 (Rozen and Skaletsky 2000). Sanger sequencing was performed by the University of Minnesota

Genomics Center. CAPS markers were developed from previously mapped SNP sequences (Close et al., 2009), and the program JoinMap 4 was used to calculate map distances (Van Ooijen, 2006).

Total RNA for sequencing (RNA-seq) was isolated from crown tissue containing the shoot apical meristem and axillary meristems from 14-day-old seedlings grown in growth chambers using the RNeasy Plant Mini Kit (Qiagen). There were three replicates of each genotype (Bowman, Bowman-*cul2.b*, Bowman-*cul2.b-rob1*, Bowman-*eli.a-17*, Bowman-*cul2.b-rob1; eli.a-17*, Bowman-*eli.a-18* and Bowman-*cul2.b-rob1; eli.a-18*), six seedlings per replicate, and tissue from each genotype was pooled. Poly A+ RNA isolation, library construction, and Illumina sequencing were performed by the University of Minnesota Genomics Center. Fragment sizes for sequencing averaged 200 base pairs (bp), after accounting for adaptor sequences, and 76 bp, paired-end reads were produced.

Relative *ELI-A* expression levels were compared in inflorescence, axillary bud, and leaf blade tissues by RT-qPCR using the procedure described by Tavakol et al. (2015). Total RNA was isolated from one cm long axillary buds from two-week-old seedlings, and five mm long inflorescences, and leaf blades from four-week-old seedlings using the Qiagen RNeasy kit (Qiagen). Approximately 250 ng of total RNA was DNase treated (RQ1 Rase-Free DNase, Promega) prior to cDNA synthesis with the ImProm-II Reverse Transcription System (Promega). One-third of the product was used for PCR. Quantitative PCR was performed on an Applied Biosystems StepOnePlus Real Time PCR System with the QuantiFast SYBR Green mix (Qiagen). *GAPDH* and *UBI* were used for normalization (Tavakol et al., 2015). Three replicates, with three to five plants each, were randomized and grown together in a growth chamber as described above. Primer sequences are shown in Supplemental Table S10.

Sequence assembly pipeline and SNP analysis

Reads for all samples were quality trimmed from both ends with custom Java code, using a base quality cutoff of Phred 20. Reads shorter than 30 bp were discarded. Trimmed reads from the Bowman sample were assembled *de novo* using the Trinity transcriptome assembler on default settings (release r2011-05-13, Grabherr et al., 2011). This resulted in a total of 31,976 transcript sequences (Supplemental Data S1).

Trimmed reads from each mutant sample were mapped separately to the Bowman Trinity transcripts using the Bowtie read mapper v. 0.12.7 (Langmead et al., 2009). To keep mismapping and the resulting false positive SNPs to a minimum, a strict mismatch rate of 1 mismatch per read was applied. Reads were mapped in “all” mode which allows multi-mappable reads to map to all of their possible mapping locations. The “--best –strata” parameter was used to ensure that only the best mapping locations were reported.

For each genotype, SNP discovery was carried out using custom-written code implemented as a prototype feature in Tablet (Milne et al., 2013). The raw variant data was then filtered using a minor allele frequency of ≥ 0.9 , to identify homozygous SNPs with the Bowman reference sequence only. Several further stages of SNP filtering followed, all of which were aimed at removing false positive SNPs. First, SNPs that were less than a read’s length from contig start or end, or regions with zero read coverage, were removed as a large proportion of these can be assumed to be artifacts caused by mis-assembly of the reference sequence (M. Bayer, unpublished data). SNPs with fewer than six instances of the alternate allele were also removed to exclude low coverage, low confidence variants. We called SNPs by mapping the Bowman reads against the Bowman Trinity assembly as a control set, on the assumption that any SNPs found in this largely homozygous cultivar must be artifacts caused by read mis-mapping or mis-assembly of the reference sequence. SNPs discovered in this dataset were subsequently removed from all of the mutant SNP sets. The remaining ‘robust SNPs’ were used for analysis.

Accession Numbers

RNAseq data have been deposited into the National Center for Biotechnology Information Short Read Archive, accession number SRP076379. *ELI-A* sequences were deposited in the National Center for Biotechnology Information database, accession numbers KU844110 - KU844117. Additional sequences mentioned in this article can be found in the GenBank, TAIR, or PlantGDB databases under the following accession numbers: GenBank/EMBL: Bradi5g04710 (XM_003581043), Bradi5g04720 (XM_003579296), CHLREDRAFT_180901 (XM_001692084), LOC_Os04g19140 (XM_015779144), LOC_Os02g25230 (XM_015767599), PP1S21_302V6 (XM_001756068), PP1S105_108V6 (XM_001768660), PP1S226_73V6 (XM_001777733), PP1S111_138V6 (XM_001769128), SELMODRAFT_231485 (XM_002969799), SELMODRAFT_10589 (XM_002985134), Si009424m.g (XM_004975201), Si016308m.g (XP_004952406), Sb04g014800 (XM_002453721), Solyc08g079550 (XM_004246091),

593 Solyc03g007180 (XM_004234118), Zm00001d004164 (XR_562337), Zm00001d025091
594 (XM_008664864), Zm00001d015889 (XM_008647228), Zm00001d053254 (XM_008681506);
595 PlantGDB: Sb06g003790.1; and TAIR: AT1G12380, AT1G62870. Original photographs used
596 for the figures have been archived at University of Minnesota Data Repository (DRUM) and can
597 be accessed at <https://doi.org/10.13020/D61H4D>.

598

599

Supplemental Materials

The following materials are available in the online version of this article.

Supplemental Tables

Supplemental Table S1. CAPS markers for *eli-a* alleles and mapping.

Supplemental Table S2. *eli-a.17*; *cul2.b-rob1* SNP list.

Supplemental Table S3. *eli-a.18*; *cul2.b-rob1* SNP list.

Supplemental Table S4. *eli-a.17* SNP list.

Supplemental Table S5. *eli-a.18* SNP list.

Supplemental Table S6. *cul2.b-rob1* SNP list

Supplemental Table S7. *cul2.b* SNP list.

Supplemental Table S8. Homologous *ELI-A* sequences in other species.

Supplemental Table S9. Plant materials.

Supplemental Table S10. PCR primer sequences.

Supplemental Figures

Supplemental Figure S1. Suppression of *cul2* by *eli-a.17* and *eli-a.18* promotes tillering.

Supplemental Figure S2. Genetic testing of *eli-a* alleles.

Supplemental Figure S3. Ligule development in *eli-a* alleles.

Supplemental Figure S4. Mapping *eli-a.17* and *eli-a.18* on chromosome 2HS.

Supplemental Figure S5. Axillary bud development in *Bowman- eli-a.18*.

Supplemental Figure S6. Rate of axillary bud and tiller appearance.

Supplemental Figure S7. *Eli-a* spike phenotypes.

Supplemental Figure S8. Secondary cell wall development in culms.

Supplemental Figure S9. Phylogenetic tree of *ELI-A* homologs.

Supplemental Figure S10. *ELI-A* expression data.

Supplemental Figure S11. *ELI-A in situ* hybridizations.

Supplemental Figure S12. Crossing scheme to develop *eli-a.17* and *Bowman-cul2.b-rob1*; *eli-a.17* families.

Supplemental Data

Supplemental Data S1. RNAseq Transcript list.

631

632

633

ACKNOWLEDGEMENTS

We thank Bruna Bucciarelli for assistance with microscopy; Gail Celio and Grant Barthel at the University Imaging Center, University of Minnesota, for help with SEM and light microscopy; Kevin Smith for providing field space, Sue Miller for assistance with RT-qPCR, Lin Li and Juan Gutierrez-Gonzalez for help with bioinformatics; The Nordic Genetic Resource Center, Harold Bockelman, the USDA National Small Grains Collection, and Andris Kleinhofs, Washington State University for providing materials; and Jerome Franckowiak for insights on the interpretation of mutants. This research was supported by a grant from the United States Department of Agriculture-CSREES-NRI Plant Growth and Development program grant # 2004-03440 and funds received from the Triticeae Coordinated Agricultural Project, US Department of Agriculture/National Institute for Food and Agriculture grant number 2011-68002-30029 to G.J.M.

Table 1. Tiller development in *eli-a.17* and *eli-a.18* mutants and in non-mutant Bowman.

Genotype	Tiller Number – 4 weeks	Tiller Number – 6 weeks	Tiller Number – maturity
Bowman ¹	7.69	28.01	33.95
Bowman- <i>eli-a.17</i> ¹	6.70	23.93*	27.37*
Bowman ²	6.61	27.32	43.99
Bowman- <i>eli-a.18</i> ²	4.73	15.75*	21.97*

¹ 2015 field

² 2016 field

* $t < 0.05$ two-tailed Student's *t*-test

Figure legends

Figure 1: Mutant and non-mutant adult plant characteristics. A, Bowman-*cul2.b-rob1*. B, Bowman-*cul2.b-rob1; eli-a.17*. C, Non-mutant Bowman cultivar. D, Bowman-*eli-a.17*. E, Bowman-*eli-a.18*. F, Bowman-*cul2.b-rob1; eli-a.18*. G, *eli-a.14*. H, *cul2.b-rob1; eli-a.14*. The non-mutant Bowman and Bowman-*eli-a.17* plants in panels C and D were grown in the field and transferred to pots for pictures. Other plants were grown in a growth chamber. Bar = 20 cm.

Figure 2: The ligular region in *eli-a* alleles. A–D, Ligules and auricles. A, Non-mutant Bowman. B, Bowman-*eli-a.17*. C, Bowman-*eli-a.18*. Note the reduced auricles at the leaf margin, indicated by the arrows and the absence of the ligule. D, Heterozygous Bowman-*eli-a.17/eli-a.18*. Note the reduced ligule and auricle development. E–F, scanning electron micrographs of the ligular regions. E, Non-mutant Bowman. The ligule has been trimmed back to uncover the underlying auricle. F, Bowman-*eli-a.18* ligular region. Scale bar = 200 μm

Figure 3. Longitudinal sections of seven-day-old shoot apices from non-mutant and mutant lines stained with Toluidine Blue. Axillary buds are shown in their own panels as median sections of the shoot apex and generally do not capture the axillary buds. A, Non-mutant Bowman shoot apical meristem. B, Bowman axillary bud #3. C, Bowman axillary bud #2. D, Bowman-*cul2.b-rob1* shoot apical meristem. E, Bowman-*eli-a.17* shoot apical meristem. F, Bowman-*eli-a.17* axillary bud. G, Bowman-*eli-a.17; cul2.b-rob1* shoot apical meristem. The edge of a small axillary bud is visible at the lower right (*). H, Section through axillary bud #1 seen in panel G. Scale bar = 100 μm .

Figure 4. Secondary cell wall development. A, Comparison of leaves from mature non-mutant Bowman and Bowman-*eli-a.18* plants. B–G are Safranin-O stained. B, Midrib from non-mutant plant. C, Midrib from Bowman-*eli-a.18* plant. D, Leaf vein from non-mutant plant. E, Leaf vein from Bowman-*eli-a.18* plant. F, Leaf margin from non-mutant plant. G, Leaf margin from

Bowman-*eli-a.18* plant. Arrows point to cell wall differences in the leaf midrib (B, C), the bundle sheath extension and mestome sheath (D, E), and the leaf margin (F, G). Scale bar = 100 μm .

Figure 5. The *ELI-A* gene and location of mutations. The dark grey box indicates the single exon in the gene and lighter grey boxes mark the 5' and 3' untranslated regions. Mutations in *eli-a.14* and *eli-a.18* created stop codons. Prediction programs Phyre², LOMETS, and InterProScan 5 identified a RNaseH-like domain at the carboxy end of the peptide.

Figure 6. *ELI-A* expression in non-mutant and *cul2.b* seedlings. A-C, Four-day-old non-mutant shoot apex probed with an antisense *ELI-A* probe. A, Longitudinal section showing little staining in or adjacent to the shoot apical meristem and axillary buds, indicated by triangles. Short patches of staining at the adaxial and abaxial sides of leaves were occasionally seen (dark arrow); this pattern is likely from vascular bundles as seen in panels B and H. Staining was observed in newly forming ligules and leaf primordia that may represent developing ligules (circled). Leaf margins were also stained (green arrow). B, Transverse section showing staining in leaf margins, midribs, and around vascular bundles. Staining along a portion of the adaxial side of a developing leaf, circled, can be followed across the leaf in serial sections, and may be associated with the developing ligules. C, Close-up view of ligule circled in panel A. D-E, four-day-old *cul2.b* shoot apex probed with an antisense *ELI-A* probe. D, Longitudinal section of a *cul2.b* shoot. E, Transverse section of a *cul2.b* shoot. *ELI-A* staining pattern was similar to non-mutant shoot apices; the variable staining in small clusters of cells along the abaxial leaf surface (arrow) was seen in non-mutant plants (Supplemental Fig. S11); transcripts were not detected in the older ligules (circled). F-G, Serial sections of four-day-old shoot probed for *ELI-A* or *HvLgl1*. F, *ELI-A* staining was observed in the same location as the adaxial *HvLgl1* staining. G, *HvLgl1* staining was detected on the adaxial and abaxial surfaces. H, *ELI-A* expression in leaf axils and axillary buds is associated with vascular bundles. Scale bar = 100 μm in panel C and 200 μm in other panels.

Parsed Citations

Ahlstrand GG (1996) Low-temperature low-voltage scanning microscopy (LTLVSEM) of uncoated frozen biological materials: a simple alternative. In: G Bailey, J Corbett, R Dimlich, J Michael, N Zaluzec, eds, *Proceedings of Microscopy Microanalysis*. San Francisco Press, San Francisco, pp 918–919

Pubmed: [Author and Title](#)

CrossRef: [Author and Title](#)

Google Scholar: [Author Only](#) [Title Only](#) [Author and Title](#)

Babb S, Muehlbauer GJ (2003) Genetic and morphological characterization of the barley unculm2 (cul2) mutant. *Theor Appl Genet* 106: 846–857

Pubmed: [Author and Title](#)

CrossRef: [Author and Title](#)

Google Scholar: [Author Only](#) [Title Only](#) [Author and Title](#)

Bar M, Ori N (2014) Leaf development and morphogenesis. *Development* 141: 4219–4230.

Pubmed: [Author and Title](#)

CrossRef: [Author and Title](#)

Google Scholar: [Author Only](#) [Title Only](#) [Author and Title](#)

Becraft PW, Bongard-Pierce DK, Sylvester AW, Poethig RS, Freeling M (1990) The liguleless-1 gene acts tissue specifically in maize leaf development. *Develop Biol* 141: 220–232

Pubmed: [Author and Title](#)

CrossRef: [Author and Title](#)

Google Scholar: [Author Only](#) [Title Only](#) [Author and Title](#)

Berger Y, Harpax-Saad S, Brand A, Melnik H, Sirding N, Alvarez JP, Zinder M, Samach A, Eshed Y, Ori N (2009) The NAC-domain transcription factor GOBLET specifies leaflet boundaries in compound tomato leaves. *Development* 136: 823–832

Pubmed: [Author and Title](#)

CrossRef: [Author and Title](#)

Google Scholar: [Author Only](#) [Title Only](#) [Author and Title](#)

Bilsborough GD, Runions A, Barkoulas M, Jenkins HW, Hasson A, et al (2011) Model for the regulation of *Arabidopsis thaliana* leaf margin development. *Proc. Natl. Acad. Sci. USA* 108: 3424–3429

Pubmed: [Author and Title](#)

CrossRef: [Author and Title](#)

Google Scholar: [Author Only](#) [Title Only](#) [Author and Title](#)

Busch BL, Schmitz G, Rossmann S, Piron F, Ding J, Bendahmane A, Theres K (2011) Shoot branching and leaf dissection in tomato are regulated by homologous gene modules. *Plant Cell* 23: 3595–3609

Pubmed: [Author and Title](#)

CrossRef: [Author and Title](#)

Google Scholar: [Author Only](#) [Title Only](#) [Author and Title](#)

Carroll SB (2008) Evo-devo and an expanding evolutionary synthesis: A genetic theory of morphological evolution. *Cell* 134: 25–36

Pubmed: [Author and Title](#)

CrossRef: [Author and Title](#)

Google Scholar: [Author Only](#) [Title Only](#) [Author and Title](#)

Close TJ, Bhat PR, Lonardi S, Wu Y, Rostoks N, Ramsay L, Druka A, Stein N, Svensson, JT, Wanamaker S, et al (2009) Development and implementation of high-throughput SNP genotyping in barley. *BMC Genomics* 10: 582.

Pubmed: [Author and Title](#)

CrossRef: [Author and Title](#)

Google Scholar: [Author Only](#) [Title Only](#) [Author and Title](#)

Dabbert T, Okagaki RJ, Cho S, Heinen S, Boddu J, Muehlbauer GJ (2010) The genetics of barley low-tillering mutants: low number of tillers-1 (Int1). *Theor Appl Genet* 121: 705–717

Pubmed: [Author and Title](#)

CrossRef: [Author and Title](#)

Google Scholar: [Author Only](#) [Title Only](#) [Author and Title](#)

Dereeper A, Guignon V, Blanc G, Audic S, Buffet S, et al (2008) Phylogeny.fr: robust phylogenetic analysis for the non-specialist. *Nucleic Acids Res* 36 (Web Server issue): W465–9

Pubmed: [Author and Title](#)

CrossRef: [Author and Title](#)

Google Scholar: [Author Only](#) [Title Only](#) [Author and Title](#)

Döring H-P, Lin J, Urig H, Salamini F (1999) Clonal analysis of the development of the barley (*Hordeum vulgare* L.) leaf using periclinal chlorophyll chimeras. *Planta* 207: 335–342

Pubmed: [Author and Title](#)

CrossRef: [Author and Title](#)

Google Scholar: [Author Only](#) [Title Only](#) [Author and Title](#)

Druka A, Franckowiak J, Lundqvist U, Bonar N, Alexander J, et al (2011) Genetic dissection of barley morphology and development.

Downloaded from on March 5, 2018 - Published by www.plantphysiol.org
Copyright © 2018 American Society of Plant Biologists. All rights reserved.

Plant Physiol 155: 617-627

Pubmed: [Author and Title](#)
CrossRef: [Author and Title](#)
Google Scholar: [Author Only Title Only Author and Title](#)

Fal K, Landrein B, Hamant O (2016) Interplay between miRNA regulation and mechanical stress for CUC gene expression at the shoot apical meristem. Plant Signal Behav 11: e1127497

Pubmed: [Author and Title](#)
CrossRef: [Author and Title](#)
Google Scholar: [Author Only Title Only Author and Title](#)

Forster BP, Franckowiak JD, Lundqvist U, Lyon J, Pitkethly I, Thomas WTB (2007) The barley phytomer. Ann Bot 100: 725-733

Pubmed: [Author and Title](#)
CrossRef: [Author and Title](#)
Google Scholar: [Author Only Title Only Author and Title](#)

Franckowiak JD, Konishi T, Lundqvist U (1997) BGS 254, Orange lemma, rob. Barley Genet Newsl 26: 235-236

Pubmed: [Author and Title](#)
CrossRef: [Author and Title](#)
Google Scholar: [Author Only Title Only Author and Title](#)

Fricke W (2002) Biophysical limitation of cell elongation in cereal leaves. Ann Bot 90: 157-167

Pubmed: [Author and Title](#)
CrossRef: [Author and Title](#)
Google Scholar: [Author Only Title Only Author and Title](#)

Gale Jr M, Blakely CM, Darveau A, Romano PR, Korth, MJ, and Katze MG (2002) P52rIPK regulates the molecular cochaperone P58IPK to mediate control of the RNA-dependent protein kinase in response to cytoplasmic stress. Biochemistry 41: 11878-11887

Pubmed: [Author and Title](#)
CrossRef: [Author and Title](#)
Google Scholar: [Author Only Title Only Author and Title](#)

Gallavotti A, Zhao Q, Kyoizuka J, Meeley RB, Ritter MK, et al (2004) The role of barren stalk1 in the architecture of maize. Nature 432: 630-635

Pubmed: [Author and Title](#)
CrossRef: [Author and Title](#)
Google Scholar: [Author Only Title Only Author and Title](#)

Grabherr MG, Haas BJ, Yassour M, Levin JZ, Thompson DA, et al (2011) Full-length transcriptome assembly from RNA-Seq data without a reference genome. Nat Biotechnol 29: 644-652

Pubmed: [Author and Title](#)
CrossRef: [Author and Title](#)
Google Scholar: [Author Only Title Only Author and Title](#)

Ha CM, Nam HG, Fletcher JC (2007) BLADE-ON-PETIOLE1 and 2 control Arabidopsis lateral organ fate through regulation of LOB domain and adaxial-abaxial polarity genes. Plant Cell 19: 1809-1825

Pubmed: [Author and Title](#)
CrossRef: [Author and Title](#)
Google Scholar: [Author Only Title Only Author and Title](#)

Hepworth SR, Pautot VA (2015) Beyond the divide: Boundaries for patterning and stem cell regulation in plants. Front Plant Sci 9: 1052

Pubmed: [Author and Title](#)
CrossRef: [Author and Title](#)
Google Scholar: [Author Only Title Only Author and Title](#)

Hickman AB, Perez ZN, Zhou L, Musingarimi P, Ghirlando R, et al (2005) Molecular architecture of a eukaryotic DNA transposase. Nat Struct Mol Biol 12: 715-721

Pubmed: [Author and Title](#)
CrossRef: [Author and Title](#)
Google Scholar: [Author Only Title Only Author and Title](#)

Humason GL (1979) Animal Tissue Techniques, Fourth Edition. W. H. Freeman and Company, San Francisco

Pubmed: [Author and Title](#)
CrossRef: [Author and Title](#)
Google Scholar: [Author Only Title Only Author and Title](#)

Javelle M, Marco CF, Timmermans M (2011) In Situ hybridization for the precise localization of transcripts in plants. J Vis Exp 57: e3328

Pubmed: [Author and Title](#)
CrossRef: [Author and Title](#)
Google Scholar: [Author Only Title Only Author and Title](#)

Johnston R, Wang M, Sun Q, Sylvester AW, Hake S, Scanlon MJ (2014) Transcriptomic analyses indicate that maize ligule development recapitulates gene expression patterns that occur during lateral organ initiation. Plant Cell 26: 4718-4732

Pubmed: [Author and Title](#)
CrossRef: [Author and Title](#)
Google Scholar: [Author Only Title Only Author and Title](#)

Keller T, Abbott J, Moritz T, Doerner P (2006) Arabidopsis REGULATOR OF AXILLARY MERISTEMS1 controls a leaf axil stem cell niche and modulates vegetative development. Plant Cell 18: 598-611

Pubmed: [Author and Title](#)

CrossRef: [Author and Title](#)

Google Scholar: [Author Only Title Only Author and Title](#)

Kelley LA, Sternberg MJE (2009) Protein structure prediction on the Web: a case study using the Phyre server. Nat Protoc 4: 363-371

Pubmed: [Author and Title](#)

CrossRef: [Author and Title](#)

Google Scholar: [Author Only Title Only Author and Title](#)

Kenzo T, Ichie T, Watanabe Y, Hiromi T (2007) Ecological distribution of homobaric and heterobaric leaves in three species of Malaysian lowland tropical rainforest. Amer J Bot 94: 764-775

Pubmed: [Author and Title](#)

CrossRef: [Author and Title](#)

Google Scholar: [Author Only Title Only Author and Title](#)

Kierzkowski D, Nakayama N, Routier-Kierzkowska A-L, Weber A, Bayer E, et al (2012) Elastic domains regulate growth and organogenesis in the plant shoot apical meristem. Science 335: 1096-1099

Pubmed: [Author and Title](#)

CrossRef: [Author and Title](#)

Google Scholar: [Author Only Title Only Author and Title](#)

Komatsu K, Maekawa M, Ujiie S, Satake Y, Furutani I, et al (2003) LAX and SPA: Major regulators of shoot branching in rice. Proc Natl Acad Sci USA 100: 11765-11770

Pubmed: [Author and Title](#)

CrossRef: [Author and Title](#)

Google Scholar: [Author Only Title Only Author and Title](#)

Langdale JA (2005) The then and now of maize leaf development. Maydica 50: 459-467

Pubmed: [Author and Title](#)

CrossRef: [Author and Title](#)

Google Scholar: [Author Only Title Only Author and Title](#)

Langmead B, Trapnell C, Pop M, Salzberg SL (2009) Ultrafast and memory-efficient alignment of short DNA sequences to the human genome. Genome Biol 10: R25

Pubmed: [Author and Title](#)

CrossRef: [Author and Title](#)

Google Scholar: [Author Only Title Only Author and Title](#)

Lee D-K, Geisler M, Springer PS (2009) LATERAL ORGAN FUSION1 and LATERAL ORGAN FUSION2 function in lateral organ separation and axillary meristem formation in Arabidopsis. Development 136: 2423-2432

Pubmed: [Author and Title](#)

CrossRef: [Author and Title](#)

Google Scholar: [Author Only Title Only Author and Title](#)

Leegood RC (2008) Roles of the bundle sheath cells in leaves of C3 plants. J Exp Bot 59: 1663-1673

Pubmed: [Author and Title](#)

CrossRef: [Author and Title](#)

Google Scholar: [Author Only Title Only Author and Title](#)

Lewis MW, Hake S (2015) Keep on growing: building and patterning leaves in the grasses. Curr Opin Plant Biol 29: 80-86

Pubmed: [Author and Title](#)

CrossRef: [Author and Title](#)

Google Scholar: [Author Only Title Only Author and Title](#)

Lundqvist U, Franckowiak JD (2002) BGS 623. Eligulum-a, eli-a. Barley Genet News 32: 124

Pubmed: [Author and Title](#)

CrossRef: [Author and Title](#)

Google Scholar: [Author Only Title Only Author and Title](#)

Majorek KA, Dunin-Horkawicz S, Steczkiewicz K, Muszewska A, Nowotny M, et al (2014) The RNase H-like superfamily: new members, comparative structural analysis and evolutionary classification. Nucl Acids Res 42: 4160-4179

Pubmed: [Author and Title](#)

CrossRef: [Author and Title](#)

Google Scholar: [Author Only Title Only Author and Title](#)

Mathan J, Bhattacharya J, Ranjan A (2016) Enhancing crop yield by optimizing plant developmental features. Development 143: 3283-3294

Pubmed: [Author and Title](#)

CrossRef: [Author and Title](#)

Google Scholar: [Author Only Title Only Author and Title](#)

Milne I, Stephen G, Bayer M, Cock JA, Pritchard L, et al (2013) Using Tablet for visual exploration of second-generation sequencing data. Brief Bioinform 14: 193-202

Downloaded from on March 5, 2018 - Published by www.plantphysiol.org
Copyright © 2018 American Society of Plant Biologists. All rights reserved.

Pubmed: [Author and Title](#)
CrossRef: [Author and Title](#)
Google Scholar: [Author Only](#) [Title Only](#) [Author and Title](#)

Moon J, Candela H, Hake S (2013) The liguleless narrow mutation affects proximal-distal signaling and leaf growth. Development 140: 405-412

Pubmed: [Author and Title](#)
CrossRef: [Author and Title](#)
Google Scholar: [Author Only](#) [Title Only](#) [Author and Title](#)

Müller D, Schmitz G, Theres K (2006) Blind homologous R2R3 Myb genes control the pattern of lateral meristem initiation in Arabidopsis. Plant Cell 18: 586-597

Pubmed: [Author and Title](#)
CrossRef: [Author and Title](#)
Google Scholar: [Author Only](#) [Title Only](#) [Author and Title](#)

Nakayama N, Smith RS, Mandel T, Robinson S, Kimura S, et al (2012) Mechanical regulation of auxin-mediated growth. Curr Biol 22: 1468-1476

Pubmed: [Author and Title](#)
CrossRef: [Author and Title](#)
Google Scholar: [Author Only](#) [Title Only](#) [Author and Title](#)

Nikovics K, Blein T, Peaucelle A, Ishida T, Morin H, Aida M, Laufs P (2006) The balance between the MIR164A and CUC2 genes controls leaf margin serration in Arabidopsis. Plant Cell 18: 2929-2945

Pubmed: [Author and Title](#)
CrossRef: [Author and Title](#)
Google Scholar: [Author Only](#) [Title Only](#) [Author and Title](#)

Oikawa T, Kyozuka J (2009) Two-step regulation of LAX PANICLE1 protein accumulation in axillary meristem formation in rice. Plant Cell 21: 1095-1108

Pubmed: [Author and Title](#)
CrossRef: [Author and Title](#)
Google Scholar: [Author Only](#) [Title Only](#) [Author and Title](#)

Quevillon E, Silventoinen V, Pillai S, Harte N, Mulder N, Apweiler R, Lopez R (2005) InterProScan: protein domains identifier. Nucleic Acids Res W116-W120

Pubmed: [Author and Title](#)
CrossRef: [Author and Title](#)
Google Scholar: [Author Only](#) [Title Only](#) [Author and Title](#)

Rozen S, Skaletsky HJ (2000) Primer3 on the WWW for general users and for biologist programmers. In: Krawetz S, Misener S (eds) Bioinformatics Methods and Protocols: Methods in Molecular Biology. Humana Press, Totowa, NJ, pp 365- 386.

Pubmed: [Author and Title](#)
CrossRef: [Author and Title](#)
Google Scholar: [Author Only](#) [Title Only](#) [Author and Title](#)

Ruzin SE (1999) Plant Microtechnique and Microscopy. Oxford University Press Inc, New York

Pubmed: [Author and Title](#)
CrossRef: [Author and Title](#)
Google Scholar: [Author Only](#) [Title Only](#) [Author and Title](#)

Schmitz G, Theres K (2005) Shoot and inflorescence branching. Curr Opin Plant Biol 8: 641-654

Pubmed: [Author and Title](#)
CrossRef: [Author and Title](#)
Google Scholar: [Author Only](#) [Title Only](#) [Author and Title](#)

Sylvester AW, Cande WZ, Freeling M (1990) Division and differentiation during normal and liguleless-1 maize leaf development. Development 110: 985-1000

Pubmed: [Author and Title](#)
CrossRef: [Author and Title](#)
Google Scholar: [Author Only](#) [Title Only](#) [Author and Title](#)

Tavakol E, Okagaki R, Verderio G, Shariati VJ, Hussien A, et al (2015) The barley Uniculme4 gene encodes a BLADE-ON-PETIOLE-like protein that controls tillering and leaf patterning. Plant Physiol 168: 164-174

Pubmed: [Author and Title](#)
CrossRef: [Author and Title](#)
Google Scholar: [Author Only](#) [Title Only](#) [Author and Title](#)

The International Barley Genome Sequencing Consortium (2012) A physical, genetic and functional sequence assembly of the barley genome. Nature 491: 711-716

Pubmed: [Author and Title](#)
CrossRef: [Author and Title](#)
Google Scholar: [Author Only](#) [Title Only](#) [Author and Title](#)

Trivett CL, Evert RF (1998) Ontogeny of the vascular bundles and contiguous tissues in the barley leaf blade. Int J Plant Sci 159: 716-723

Pubmed: [Author and Title](#)
CrossRef: [Author and Title](#)
Google Scholar: [Author Only](#) [Title Only](#) [Author and Title](#)

Van Ooijen JW (2006) JoinMap® 4, Software for the calculation of genetic linkage maps in experimental populations. Kyazma B V, Wageningen, Netherlands

Pubmed: [Author and Title](#)
CrossRef: [Author and Title](#)
Google Scholar: [Author Only](#) [Title Only](#) [Author and Title](#)

Walsh J, Waters CA, Freeling M (1998) The maize gene liguleless2 encodes a basic leucine zipper protein involved in the establishment of the leaf blade-sheath boundary. Genes & Develop 12: 208-218

Pubmed: [Author and Title](#)
CrossRef: [Author and Title](#)
Google Scholar: [Author Only](#) [Title Only](#) [Author and Title](#)

Wang Q, Hasson A, Rossmann S, Theres K (2016) Divide et impera boundaries shape the plant body and initiate new meristems. New Phytologist 209: 485–498

Pubmed: [Author and Title](#)
CrossRef: [Author and Title](#)
Google Scholar: [Author Only](#) [Title Only](#) [Author and Title](#)

Wang Y, Li J (2008) Molecular basis of plant architecture. Ann Rev Plant Biol 59: 253-279

Pubmed: [Author and Title](#)
CrossRef: [Author and Title](#)
Google Scholar: [Author Only](#) [Title Only](#) [Author and Title](#)

Wenzel CL, Chandler PM, Cunningham RB, Passioura JB (1997) Characterization of the leaf epidermis of barley (Hordeum vulgare L. 'Himalaya'). Annals Bot 79: 41-46

Pubmed: [Author and Title](#)
CrossRef: [Author and Title](#)
Google Scholar: [Author Only](#) [Title Only](#) [Author and Title](#)

Wu S, Zhang Y (2007) LOMETS: A local meta-threading-server for protein structure prediction. Nucl Acids Res 35: 3375-3382

Pubmed: [Author and Title](#)
CrossRef: [Author and Title](#)
Google Scholar: [Author Only](#) [Title Only](#) [Author and Title](#)

Yang F, Wang Q, Schmitz G, Müller D, Theres K (2012) The bHLH protein ROX acts in concert with RAX1 and LAS to modulate axillary meristem formation in Arabidopsis. Plant J 71: 61-70

Pubmed: [Author and Title](#)
CrossRef: [Author and Title](#)
Google Scholar: [Author Only](#) [Title Only](#) [Author and Title](#)

Žádníková P, Simon R (2014) How boundaries control plant development. Curr Opin Plant Biol 17: 116-125

Pubmed: [Author and Title](#)
CrossRef: [Author and Title](#)
Google Scholar: [Author Only](#) [Title Only](#) [Author and Title](#)